Springer

Journal of
Mechanical
Science and
Technology

Journal of Mechanical Science and Technology 22 (2008) 1349~1358

www.springerlink.com/content/1738-494x

Identification of impact force in thick plates based on the elastodynamics and time-frequency method (I)

-Theoretical approach for identification the impact force based on elastodynamics-

Sang Kwon Lee*

Department of Mechanical Engineering, Inha University, Incheon, 402-751, Korea

(Manuscript Received January 14, 2008; Revised March 27, 2008; Accepted March 31, 2008)

Abstract

Determination of impact load is important for detecting and analyzing the flaws in thick plate. In industrial plants, thick aluminum plate is popularly used and impact load is identified by convolving the acoustic waveform, which is measured with sensors arrayed on the plate, and by Green's function, which is the transfer function between impacting position and sensor. In practical situations, it is difficult to measure Green's function. In this paper, the impact load on the plate is inversely recovered by using Green's function and the acoustic waveform. Green's function and the acoustic waveform are theoretically obtained based on the plate theory. There are three plate theories. One is the classic plate theory (CPT), which has been used for thin plate. The others are the exact plate theory and the approximated shear deformation theory (SDPT), which are used for the thick plate because the CPT overestimates the group velocity at high frequency in the thick plate. In this paper, the thick plate theory is used for the prediction of the acoustic waveform. This theoretical Green's function can be also used for the inverse problem of impact load based on the experimental method.

Keywords: Thick plate; Green's function; Group velocity; Inverse force; Non-destructive; Wave motion

1. Introduction

Elastic plates have been extensively used in aircraft, aerospace, automotive, industrial plant and power plants. One of major concerns in these plate structures is the damage due to impact loads. For instance, a low-velocity impact can cause delamination inside composite structures. If undetected, the damage can grow, leading to catastrophic failure of the structure. Therefore, a system that can detect the impact location and estimate the amount of impact energy would be very helpful in the health monitoring of structures. In general, the analysis of structures subject to dynamic loads can be categorized into three basic problems: (a) given the input and the system parameters, determine the output, (b) given the input and the output, determine the system parameters, and (c) given the system parameters and the output, determine the input. While problems of the first category are described as direct problems, the second and third types are inverse problems. Inverse problems are of great current interest in a variety of applications and they have been investigated extensively by many authors [1-5]. Therefore, a system that can detect the location of impact and estimate its energy can be very helpful in developing health-monitoring systems for advanced structures. Michael and Pao [1] developed a method that determined a dynamic force by using wave motion measurement. In this case the location of the impact load was known. In many impact load problems, however, the location of impact load is generally not known. Therefore, in order to identify the location of impact load, various methods are investigated. In the acoustic emission technique, the standard method of planar source location is to place

*Corresponding author. Tel.: +82 32 860 7305, Fax.: +82 32 868 1716
E-mail address: sangkwon@inha.ac.kr
DOI 10.1007/s12206-008-0319-7

three or more transducers on the surface of elastic plate and triangulate the source position by using the differences in arriving times of the acoustic wave at sensors [6-8]. After the location of impact load is detected, a theoretical solution to impact load is used for the determination of impact energy. Gaul and Hurlebaus adapt the classic plate theory (CPT) as a theoretical solution to an impact load after identification of the location of impact load [2]. In determining the impact energy, there are different approach methods [3, 4]. These methods are based on structure model to predict the response to impact load. These models characterize the relation between the input and the sensor output. The response comparator compares the measured sensor signal with the predicted model. Sensors are arrayed on the plate. One method used the strain gauges as sensors [3]. The other used the piezoelectric film as sensors [4]. These methods used the classic plate theory as a prediction model predicting the response to an impact load in the structure model. If the thickness of elastic plate is small, a sufficiently accurate response can often obtained through class plastic theory. However, a full elastodynamic theory (it is called the exact solution) needs to be employed in the solution of the problem in order to obtain meaningful results or the approximate SDPT; where the transverse shear and rotary inertia are retained in the modeling the dynamic deformations across the thickness of plate, should be used [9, 10]. In general, because of being computationally intensive, the approximate SDPT, instead of the exact solution, can be used [11]. In this study, an advanced experimental method, the theoretical method is presented to determine the impact force based on the theoretical Green's function and the simulated waveform based on either the exact plate theory or the approximate SDPT for the plate as shown in Fig. 1.

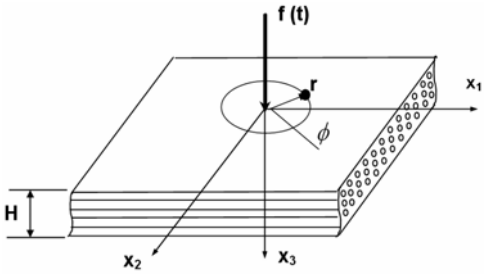

Fig. 1. Geometry of point load problem.

2. Theory of impact load in plate

Many researchers have extensively researched the theoretical solution to the surface load on the plate. Green's function in an infinite plate needed for this study can also be solved by exact plate theory, approximate SDPT, but the CPT is not employed since it is well known that the classical plate bending theory of the plate underestimates the deflections as well as the stresses and overestimates the phase velocity of the propagating waves. The plate used for theoretical model is composite laminates as shown in Fig. 1. This model is used for the identification of impact load in a thick isotropic plate in this study.

2.1. Theory of elastodynamics

The behavior of elastic waves propagating through a composite material is determined by its elastic properties. Composite materials are known to be strong dissipative. For fiber–reinforced composites, dissipation of the waves is caused by the viscoelastic nature of the resin and by scattering from the fibers and other in homogeneities. Both effects can be modeled in the frequency domain by assuming that the stiffness constants, C_{ij} are complex and frequency dependent. A possible form of C_{ij} that can be modeled by the essential features of the dissipation caused by these factors has been given in Mal and Bar-Cohen [12] and will be used here. Assuming that the symmetry is along the x_1-axis the constitutive relation for the orthotropic material can be expressed in the frequency domain in the form [13].

$$\begin{Bmatrix} \bar{\sigma}_{11} \\ \bar{\sigma}_{22} \\ \bar{\sigma}_{33} \\ \bar{\sigma}_{23} \\ \bar{\sigma}_{31} \\ \bar{\sigma}_{12} \end{Bmatrix} = \begin{bmatrix} C_{11} & C_{12} & C_{12} & 0 & 0 & 0 \\ C_{12} & C_{22} & C_{23} & 0 & 0 & 0 \\ C_{12} & C_{23} & C_{22} & 0 & 0 & 0 \\ 0 & 0 & 0 & C_{44} & 0 & 0 \\ 0 & 0 & 0 & 0 & C_{55} & 0 \\ 0 & 0 & 0 & 0 & 0 & C_{55} \end{bmatrix} \begin{Bmatrix} \bar{u}_{1,1} \\ \bar{u}_{2,2} \\ \bar{u}_{3,3} \\ \bar{u}_{2,3} + \bar{u}_{3,2} \\ \bar{u}_{1,3} + \bar{u}_{3,1} \\ \bar{u}_{1,2} + \bar{u}_{2,1} \end{Bmatrix} \tag{1}$$

where $\bar{\sigma}_{ij}$ is the (Fourier time) transform of

Cauchy's stress tensor, $\overline{u}_i$ is the transform of displacement components, C_{44} = (C_{22} - C_{23})/2 and the five independent stiffness constants of the material are C_{11}, C_{12}, C_{22}, C_{23} and C_{55}. Modeling the effective elastic moduli of composite materials has been the topic of many studies. For low frequencies and low fiber concentration, the theoretical prediction of the effective elastic constants is in good agreement with experimental results. On the other hand, for high frequencies the theoretical estimates are not satisfactory since the effect of wave scattering by the fibers becomes significant. For fiber-reinforced composite materials, dissipation of the waves is caused by the viscoelastic nature of the resin and by multiple scattering from the fibers as well as other inhomogeneities. Both of these effects can be modeled by assuming complex and frequency-dependent stiffness constants, C_{ij}, in the form [12].

$$C_{11} = \frac{c_{11}}{1 + ip\sqrt{c_{55}/c_{11}}}, \quad C_{22} = \frac{c_{22}}{1 + ip\sqrt{c_{55}/c_{22}}},$$
$$C_{12} + C_{55} = \frac{c_{12} + c_{55}}{1 + ip\sqrt{c_{55}/(c_{12} + c_{55})}} \tag{2a}$$
$$C_{44} = \frac{C_{22} - C_{23}}{2} = \frac{c_{44}}{1 + ip\sqrt{c_{55}/c_{44}}}, \quad C_{55} = \frac{c_{55}}{1 + ip}$$

where c_{ij} is the real, perfectly elastic stiffness constant and p is the damping factor which can be expressed in the form,

$$p = p_0[1 + a_0(\frac{\omega}{\omega_0} - 1)^2 H(\frac{\omega}{\omega_0} - 1)] \tag{2b}$$

The parameter p_0 represents the effect of material dissipation, a_0 models the effect of scattering due to the fibers and other inhomogeneities, and ω_0 is a frequency below which the scattering effect is negligible. For multilayered laminates, each layer is assumed to be transversely isotropic, with its own axis of symmetry along the fibers, and is bonded to its neighbors with a thin layer of the matrix material. In the present analysis, these interfacial layers are ignored for the sake of simplicity, but if needed, they can be incorporated in the analysis without difficulty.

2.2. Exact solution for impact load

We introduce Fourier time transforms of all time-dependent variables f through

$$f(x_1, x_2, t) = \mathrm{Re}\frac{1}{\pi}\int_0^\infty \hat{f}(x_1, x_2, \omega)e^{-i\omega t}d\omega \tag{3a}$$

$$\hat{f}(x_1, x_2, \omega) = \int_0^\infty f(x_1, x_2, t)e^{i\omega t}dt \tag{3b}$$

and denote the Fourier time transform of displacement and stress component u_i $(x,t), \sigma_{ij}$ (x,t) by $\hat{u}_i(x,\omega), \hat{\sigma}_{i,j}(x,\omega)$. Then, under the assumption of initial rest, $\hat{u}_i(x,\omega), \hat{\sigma}_{i,j}(x,\omega)$ are the solution of the system

$$\hat{\sigma}_{ij,j} + \rho\omega^2\hat{u}_i = 0 \tag{4}$$
$$\hat{\sigma}_{\alpha 3}(x_1, x_2, 0, \omega) = 0, (\alpha = 1, 2) \tag{5a}$$
$$\hat{\sigma}_{33}(x_1, x_2, 0, \omega) = -\hat{f}(\omega)\delta(x_1)\delta(x_2) \tag{5b}$$
$$\hat{\sigma}_{i3}(x_1, x_2, H, \omega) = 0 \tag{5c}$$

where the applied load $f(t)$ is assumed to be concentrated at the origin on the top surface of the plate and $\hat{f}(\omega)$ is its Fourier time transform. The Cauchy's equation of motion (4) must be supplemented by the constitutive Eq. (1), and the solution must satisfy the outgoing wave condition at large lateral distance from the load. In order to obtain a formal solution of the boundary value problem in the frequency domain, we introduce double spatial Fourier transforms of $\hat{u}_i(x,\omega)$ and $\hat{\sigma}_{i,j}(x,\omega)$ through

$$\hat{u}_i(x_1, x_2, x_3, \omega) = \frac{1}{4\pi^2}\int_{-\infty}^{\infty}\int_{-\infty}^{\infty} U_i(\xi_1, \xi_1, x_3, \omega)e^{j(\xi_1 x_1 + \xi_2 x_2)}d\xi_1 d\xi_2 \tag{6a}$$
$$\hat{\sigma}_i(x_1, x_2, x_3, \omega) = \frac{1}{4\pi^2}\int_{-\infty}^{\infty}\int_{-\infty}^{\infty} \Sigma_{ij}(\xi_1, \xi_1, x_3, \omega)e^{j(\xi_1 x_1 + \xi_2 x_2)}d\xi_1 d\xi_2 \tag{6b}$$

where $\hat{u}_i(x_1, x_2, x_3, \omega)$ is the i^{th} directional Green's function $\hat{g}^u_{ij}(x_1, x_2, x_3, \omega)$ on the top of the plate due to impact force $f(t) = \delta(t)$ at the origin. Substitution from Eq. (9a,b) into Eq. (7) and Eq. (8) leads to a two-point boundary value problem of a system of ordinary differential equations for $U_i(x_3)$ which can in principle be solved. To this end, it is convenient to introduce the six dimensional "stress-displacement vector" $\{S\}$ in the transformed domain, defined by

$$\{S(x_3)\} = \{U_i(x_3) \quad \Sigma_{i3}(x_3)\} \tag{7}$$

$\{S\}$ can be expressed in a partitioned matrix product form as [14].

$$\{S(x_3)\} = \begin{bmatrix} Q_{11} & Q_{12} \\ Q_{21} & Q_{22} \end{bmatrix} \begin{bmatrix} E^+(x_3) & 0 \\ 0 & E^-(x_3) \end{bmatrix} \begin{Bmatrix} C^+ \\ C^- \end{Bmatrix} \quad (8)$$

where

$$E^+(x_3) = \text{diag}[e^{j\varsigma_1 x_3} e^{j\varsigma_2 x_3} e^{j\varsigma_3 x_3}] \quad (9a)$$

$$E^-(x_3) = \text{diag}[e^{j\varsigma_1 (H-x_3)} e^{j\varsigma_2 (H-x_3)} e^{j\xi_3 (H-x_3)}] \quad (9b)$$

$$\{C^\pm\} = \{c_i^\pm\} \quad (9c)$$

In the above, $c_i^\pm$ are complex constants related to downgoing and upgoing waves within the laminate, $[Q_{ij}]$ are 3×3 matrices, and ζ_i are the "vertical" wave numbers of the three possible waves in the composite with "horizontal" wave number ξ_1, ξ_2. The expressions for $[Q_{ij}]$ are given by

$$[Q_{11}] = \begin{bmatrix} j\xi_1 q_{11} & j\xi_1 q_{12} & 0 \\ j\xi_2 q_{21} & j\xi_2 q_{22} & j\xi_3 \\ j\xi_1 q_{21} & j\xi_2 q_{22} & -j\xi_2 \end{bmatrix} \quad (10a)$$

$$[Q_{12}] = \begin{bmatrix} j\xi_1 q_{11} & j\xi_1 q_{12} & 0 \\ j\xi_2 q_{21} & j\xi_2 q_{22} & -j\xi_3 \\ -j\xi_1 q_{21} & -j\xi_2 q_{22} & -j\xi_2 \end{bmatrix} \quad (10b)$$

$$[Q_{22}] \quad (10c)$$

$$= \begin{bmatrix} \rho A_5 \xi_1 \zeta_1 (q_{11} + q_{21}) & \rho A_5 \xi_1 \zeta_2 (q_{12} + q_{22}) & \rho A_5 \xi_1 \xi_2 \\ 2\rho A_4 \xi_2 \zeta_1 q_{21} & 2\rho A_4 \xi_2 \zeta_2 q_{22} & \rho A_4 (\xi_2^2 - \zeta_3^2) \\ \delta_1 & \delta_2 & -2\rho A_4 \xi_2 \zeta_3 \end{bmatrix} \quad (10d)$$

where

$$A_1 = C_{22}/\rho,\ A_2 = C_{11}/\rho,\ A_3 = (C_{12} + C_{55})/\rho,$$
$$A_4 = C_{44}/\rho,\ A_5 = C_{55}/\rho, \quad (11)$$

$$\delta_1 = \rho\left[\left(A_5 - A_3\right)\xi_1^2 q_{11} - \left(A_1 - 2A_4\right)\xi_2^2 q_{21} - A_1 \zeta_1^2 q_{21}\right] \quad (12a)$$

$$\delta_2 = \rho\left[\left(A_5 - A_3\right)\xi_1^2 q_{12} - \left(A_1 - 2A_4\right)\xi_2^2 q_{22} - A_1 \zeta_1^2 q_{22}\right] \quad (12b)$$

And

$$q_{11} = A_3 b_1, \quad (13a)$$

$$q_{21} = \omega^2 - A_2 \xi_1^2 - A_5 b_1, \quad (13b)$$

$$q_{12} = A_3 b_1, \quad (13c)$$

$$q_{22} = \omega^2 - A_2 \xi_1^2 - A_5 b_1, \quad (13d)$$

where

$$b_1 = -\left(\frac{\beta}{2\alpha}\right) - \sqrt{\left(\frac{\beta}{2\alpha}\right)^2 - \frac{\gamma}{\alpha}} \quad (14a)$$

$$b_2 = -\left(\frac{\beta}{2\alpha}\right) + \sqrt{\left(\frac{\beta}{2\alpha}\right)^2 - \frac{\gamma}{\alpha}} \quad (14b)$$

$$\alpha = A_1 A_5, \quad (15a)$$

$$\beta = (A_1 A_2 + A_5^2 - A_3^2)\xi_1^2 - \omega^2 (A_1 + A_5) \quad (15b)$$

$$\gamma = \left(A_2 \xi_1^2 - \omega^2\right)\left(A_5 \xi_1^2 - \omega^2\right) \quad (15c)$$

$$\zeta_1^2 = -\xi_2^3 + b_1 \quad (16a)$$

$$\zeta_2^2 = -\xi_2^3 + b_2 \quad (16b)$$

$$\zeta_3^2 = -\xi_2^2 + (\omega^2 - A_5 \xi_1^2)/A_4 \quad (16c)$$

subject to $\text{Im}(\zeta_j) \geq 0, j = 1,2,3$. The six constants must be determined from the boundary conditions (5b,c), which can be restated in the spatial transform domain as

$$\{S(0)\} = \{U_i(0) \quad \Sigma_{i3}(0)\} \quad (17a)$$

$$\{S(H)\} = \{U_i(H) \quad \Sigma_{i3}(H)\} \quad (17b)$$

where

$$\{\Sigma_{i3}(0)\} = \{0, \quad 0, \quad -\hat{f}(\omega)\} \quad (18a)$$

$$\{\Sigma_{i3}(H)\} = \{0, \quad 0, \quad 0\} \quad (18b)$$

The use of Eq. (8) in Eq. (17a,b) leads to the following system of equations for the 12 unknowns, $\{c_i^\pm\}, \{U_i(0)\}$, and $\{U_i(H)\}$,

$$\begin{bmatrix} Q_{11} & Q_{12} \\ Q_{21} & Q_{22} \end{bmatrix} \begin{bmatrix} I & 0 \\ 0 & E(H) \end{bmatrix} \begin{Bmatrix} C^+ \\ C^- \end{Bmatrix} = \begin{Bmatrix} U(0) \\ \Sigma(0) \end{Bmatrix} \quad (19a)$$

$$\begin{bmatrix} Q_{11} & Q_{12} \\ Q_{21} & Q_{22} \end{bmatrix} \begin{bmatrix} E(H) & 0 \\ 0 & I \end{bmatrix} \begin{Bmatrix} C^+ \\ C^- \end{Bmatrix} = \begin{Bmatrix} U(H) \\ \Sigma(H) \end{Bmatrix} \quad (19b)$$

where [I] is the 3×3 identify matrix,

$$E\ (H) = \text{diag}[e^{j\varsigma_1 H} e^{j\varsigma_2 H} e^{j\varsigma_3 H}] \quad (20)$$

and we have used the notation

$$\{U\} = \{U_i\},\ \{\Sigma\} = \{\Sigma_i\} \quad (21)$$

Eqs. (19a,b) can be solved to yield

$$\left\{C^{+}\right\}=\left[Q_{21}-Q_{22}EQ_{22}^{-1}EQ_{21}E\right]^{-1}\left\{\Sigma(0)-[Q_{22}EQ_{22}^{-1}]\Sigma(H)\right\} \quad (22a)$$

$$\left\{C^{-}\right\}=[Q_{22}^{-1}]\{\Sigma(H)\}-\left[Q_{22}^{-1}Q_{21}E\right]\left\{C^{+}\right\} \quad (22b)$$

$$\{U(0)\}=[Q_{11}]\left\{C^{+}\right\}+[Q_{12}E]\left\{C^{-}\right\} \quad (22c)$$

$$\{U(H)\}=[Q_{11}E]\left\{C^{+}\right\}+[Q_{12}]\left\{C^{-}\right\} \quad (22d)$$

In view of Eq. (14b), we have

$$\{U(0)\}=\left[Q_{11}-Q_{12}EQ_{22}^{-1}Q_{21}E\right]\left[Q_{21}-Q_{22}EQ_{22}^{-1}Q_{21}E\right]^{-1}\{\Sigma(0)\} \quad (23a)$$

$$\{U(H)\}=\left[Q_{11}-Q_{12}EQ_{22}^{-1}Q_{21}\right]\left[E\right]\left[Q_{21}-Q_{22}EQ_{22}^{-1}Q_{22}E\right]^{-1}\{\Sigma(0)\} \quad (23b)$$

where

$$\{\Sigma(0)\}=-\hat{f}(\omega)\{0,\quad 0,\quad 1\} \quad (24)$$

In case of a uniform half-space, $H\to\infty$, $\{E\}=[0]$ and from Eq. (23a),

$$\{U(0)\}=\left[Q_{11}Q_{21}^{-1}\right]\{\Sigma(0)\} \quad (25)$$

Eqs. (23a,b) give the transformed surface displacement and Eq. (8) can then be used to obtain the transformed displacement and stress components in the interior of the plate. The Fourier time-transformed displacements and stresses are given by the double integral expressions (6a,b).

2.3. Approximate solution for impact load

If the thickness of the laminate, H, is much smaller than the wavelengths, then the problem can be solved by approximate methods. It is well known that the classical plate bending theory of the plate underestimates the deflections as well as the stresses and overestimates the phase velocity of the propagating waves. The classical theory becomes more and more inaccurate at higher frequencies. Refined higher order theories have been developed by many authors in an effort to improve the accuracy of the approximate results [11]. The first order shear deformation plate theory (SDPT) retaining transverse shear and rotary inertia of the plate elements is used here. Assuming that the *xy*-plane is the mid-plane of the laminate, the displacement components within the laminate are assumed to be of the form,

$$\begin{aligned} u(x,y,z,t)&=u_0(x,y,t)+z\psi_x(x,y,t)\\ v(x,y,z,t)&=v_0(x,y,t)+z\psi_y(x,y,t)\\ w(x,y,z,t)&=w_0(x,y,t)\end{aligned} \quad (26)$$

where (u_0, v_0, w_0) are the displacement components at a point in the mid-plane, and ψ_x and ψ_y are the rotations of a line element, originally perpendicular to the longitudinal plane, about the y and x axes, respectively. The governing equations for the out of plane displacement for the point load problem can be expressed in the form:

$$A_{55}\frac{\partial}{\partial x}\left(\psi_x+\frac{\partial w_0}{\partial x}\right)+A_{44}\frac{\partial}{\partial x}\left(\psi_y+\frac{\partial w_0}{\partial y}\right)-\rho H\frac{\partial^2 w_0}{\partial^2 t}=-f(t)\delta(x)\delta(y) \quad (27a)$$

$$\frac{\partial}{\partial x}\left(D_{11}\frac{\partial\psi_x}{\partial x}+D_{12}\frac{\partial\psi_y}{\partial y}\right)+D_{55}\frac{\partial}{\partial y}\left(\frac{\partial\psi_x}{\partial y}+\frac{\partial\psi_y}{\partial x}\right)-A_{55}\frac{\partial}{\partial y}\left(\psi_x+\frac{\partial w_0}{\partial x}\right)-\frac{\rho H^3}{12}\frac{\partial^2\psi_x}{\partial^2 t}=0 \quad (27b)$$

$$D_{55}\frac{\partial}{\partial x}\left(\frac{\partial\psi_x}{\partial y}+\frac{\partial\psi_y}{\partial x}\right)+\frac{\partial}{\partial y}\left(D_{12}\frac{\partial\psi_x}{\partial x}+D_{22}\frac{\partial\psi_y}{\partial y}\right)-A_{44}\frac{\partial}{\partial y}\left(\psi_y+\frac{\partial w_0}{\partial y}\right)-\frac{\rho H^3}{12}\frac{\partial^2\psi_y}{\partial^2 t}=0 \quad (27c)$$

where

$$A_{ij}=P_{ij}H, D_{ij}=P_{ij}H^3/12 \quad (28a)$$

$$P_{11}=C_{11}-C_{12}^2/C_{22},\quad P_{12}=C_{12}(1-C_{23}/C_{22}) \quad (28b)$$

$$P_{22}=C_{22}-C_{23}^2/C_{22}, P_{55}=C_{55} \quad (28c)$$

The solution of these equations can be obtained by the transform technique in the form

$$\hat{\psi}_x(x,y,\omega)=\frac{1}{4\pi^2}\int_{-\infty}^{\infty}\int_{-\infty}^{\infty}\psi_x(\xi_1,\quad \xi_2,\quad \omega)e^{j(\xi_1 x+\xi_2 y)}d\xi_1 d\xi_2 \quad (29a)$$

$$\hat{\psi}_y(x,y,\omega) = \frac{1}{4\pi^2}\int_{-\infty}^{\infty}\int_{-\infty}^{\infty}\psi_y(\xi_1,\ \xi_2,\ \omega)e^{j(\xi_1 x+\xi_2 y)}d\xi_1 d\xi_2 \quad (29b)$$

$$\hat{w}_0(x,y,\omega) = \frac{1}{4\pi^2}\int_{-\infty}^{\infty}\int_{-\infty}^{\infty}W_0(\xi_1,\ \xi_2,\ \omega)e^{j(\xi_1 x+\xi_2 y)}d\xi_1 d\xi_2 \quad (29c)$$

where $\hat{\psi}_x(x,y,\omega)$, $\hat{\psi}_y(x,y,\omega)$, $\hat{w}_0(x,y,\omega)$ are the Fourier time transforms of $\psi_x(x,y,t)$, $\psi_y(x,y,t)$, $w_0(x,y,t)$, respectively. When the surface load $f(t)$ is delta function $\delta(t)$ at origin 0, the displaced $\hat{w}_0(x_1,x_2,x_3,\omega)$ is Green's function displacement $\hat{g}_{ij}^{u}(x_1,x_2,x_3,\omega)$. The unknown functions W_0, ψ_x ψ_y satisfy the system of linear equations

$$[\mathbf{M}]\{\mathbf{V}\}=\{\mathbf{F}\} \quad (30)$$

where $\{\mathbf{V}\} = \{W_0, \psi_x \psi_y\}$, $\{\mathbf{F}\} = \{-1, 0, 0\}$ and the matrix $[\mathbf{M}]$ is given by

$$[\mathbf{M}] = \begin{bmatrix} -(A_{55}\xi_1^2 + A_{44}\xi_2^2 - \rho H\omega^2) & A_{55}\xi_1 j & A_{44}\xi_2 j \\ A_{55}\xi_1 j & D_{11}\xi_1^2 + D_{55}\xi_2^2 + A_{55} - \frac{\rho H^3}{12}\omega^2 & (D_{12}+D_{55})\xi_1\xi_2 \\ A_{44}\xi_2 j & (D_{12}+D_{55})\xi_1\xi_2 & D_{22}\xi_2^2 + D_{55}\xi_1^2 + A_{44} - \frac{\rho H^3}{12}\omega^2 \end{bmatrix} \quad (31)$$

2.4 Recovery of impact load

In the plate as shown in Fig. 1, the source is located at $\mathbf{r}^0 = (0,0,0)$ and a receiver is at $\mathbf{r} = (x_1,x_2,x_3)$, where H is the plate thickness. It is assumed that it can be modeled as infinite in extent. The Green's function displacement, $g_{ij}^{u}(\mathbf{r},\ t : \mathbf{r}^0)$, is defined to be the displacement response in the i^{th} direction at $\mathbf{r}$ and t due to an impulsive concentrated force of unit magnitude in the j^{th} direction at $\mathbf{r}^0$ and $t = 0$. Green's function displacement tensor g_{ij}^{a} is given by differentiating g_{ij}^{u}. Thus, for a point force $f_j(\mathbf{r}^0,t)$ acting at $\mathbf{r}^0$ that is zero for $t<0$, the resulting displacement is,

$$u_i(\mathbf{r},t) = \sum_{j=1}^{3}\int_0^t g_{ij}^{u}(\mathbf{r},t-\tau : \mathbf{r}^0)f_j(\mathbf{r}^0,\tau)d\tau = \sum_{j=1}^{3} g_{ij}^{u}(\mathbf{r},t : \mathbf{r}^0) * f_j(\mathbf{r}^0,t) \quad (32)$$

where the asterisk denotes a convolution integral in the time variable. According to linear system theory, the Fourier transform version of displacement is given by,

$$\hat{u}_i(\mathbf{r},\omega) = \sum_{j=1}^{3}\hat{g}_{ij}^{u}(\mathbf{r},\omega;\mathbf{r}^0)\times\hat{f}_j(\mathbf{r}^0,\omega) \quad (33)$$

When acceleration is used, it is expressed as follows:

$$\hat{a}_i(\mathbf{r},\omega) = \sum_{j=1}^{3}\hat{g}_{ij}^{a}(\mathbf{r},\omega;\mathbf{r}^0)\times\hat{f}_j(\mathbf{r}^0,\omega) \quad (34)$$

The Fourier transform version of impact load is estimated by,

$$\hat{f}_i(\mathbf{r}^0,\omega) = \sum_{j=1}^{3}\hat{g}_{ij}^{a}(\mathbf{r},\omega;\mathbf{r}^0)\times\hat{a}_j(\mathbf{r},\omega) \quad (35)$$

The time history of impact load is obtained by inverse Fourier transforms of $\hat{f}_j(\omega)$. In this paper, the direction of force is the only vertical.

2.5. Numerical results

A major objective of this paper is to determine the impact force throughout measurement of the acoustic signal at the arbitrary point r in the plate as shown in Fig. 1. In order to do Green's function between impact point and the arbitrary point r is required. Green's function is a impulse response function at point r when impact force $f(t)$ is delta function $\delta(t)$. The material property of the aluminum plate used for this numerical analysis is given by Table 1. The phase velocity of this plate is calculated with exact plate theory [15], Mindlin's approximate SDPT theory [9], and CPT theory [16]. For isotropic aluminum plate,

$$C_{22} = C_{22} = C_{33} = \lambda + 2\mu \quad (36a)$$

$$C_{12}=C_{13}=C_{23} = \lambda \quad (36b)$$

and

Table 1. Material properties.

Aluminum plate	
Young's Modulus (E)	70Gpa
Poisson's ratio (ν)	0.3
Density (ρ)	2760kg/m^3
Thickness(H)	10mm

$$C_{44} = C_{55} = C_{66} = \mu \tag{36c}$$

where the constants λ and μ are known as Lame constants. These can be expressed in terms of Young' modulus E and Poisson's ratio ν [13]. Fig. 2 shows dispersive curves for the multi mode of the aluminum plate. The phase velocity of A0 flexible mode is compared with the phase velocity obtained by using the SDPT and the CPT. These results are illustrated in Fig. 3. From these results, it is confirmed that the classical plate bending theory of the plate overestimates the phase velocity of the propagating waves. The phase velocity using SDPT is the same as the phase velocity of dispersive A0 mode obtained by using exact solution. The group velocity using exact solution is obtained by calculating slope of angular frequency (ω) verse wave number (ξ) [15].

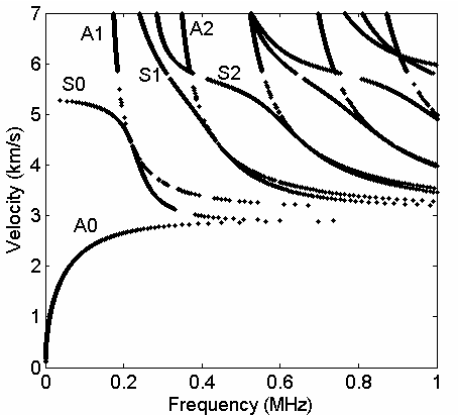

Fig. 2. Dispersive curve for the multi mode of aluminum plate.

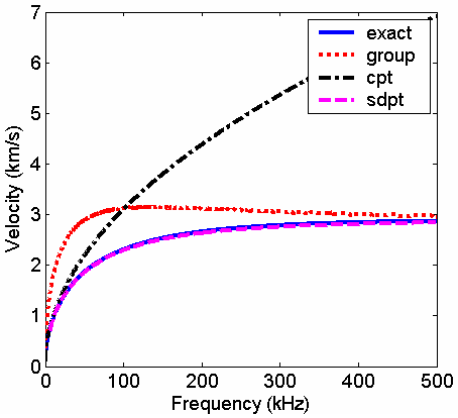

Fig. 3. Comparison of propagation wave velocity for a flexible wave in an aluminum plate.

$$C_g = \frac{d\omega}{d\xi} = \frac{c_p}{1 - \frac{\omega}{c_p}\frac{dc_p}{d\omega}} \tag{37}$$

where c_p is phase velocity and ω is angular velocity. Fig. 4 shows the comparison between Green's function displacement g_{ij}^{u} between r=0 and r =200mm obtained by using exact solution and that by using SPDT in aluminum plate. The top plot is non-filtered Green's functions. Bottom plot is Green's functions filtered by a Butterworth band pass filter from 2,000Hz to 4,000Hz. In this case, sampling frequency was 81,920Hz. According to dispersive curves as shown in Fig. 2, up to this sampling frequency, the A0 antisymmetric flexible mode and S0 symmetric modes overrule the wave propagation in plate. Therefore, the non-filtered Green's functions can be affected by S0 Lamb modes in exact solution and its shape is different with that obtained by using SDPT. However, at lower frequency, the filtered Green's function in exact solution is exactly the same as Green's function in SPDT because at this frequency the dispersive curve is affecting only the A0 mode. Fig. 5 also shows a comparison between Green's function at r = 200mm obtained by using exact solution and that by using SPDT in aluminum plate. In this case, sampling frequency was 4,096,000Hz. The top plot is non-filtered Green's functions. Bottom plot is Green's functions filtered by a Butterworth band pass filter from 10,000Hz to 200,000Hz. According to dispersive curves as shown in Fig. 2, up to this sampling frequency, the many antisymmetric flexible modes and symmetric modes overrule the wave propagation in plate. Therefore, the non-filtered Green's functions can be affected by many Lamb modes in exact solution and its shape is different with the shape of Green's function obtained by using SDPT. However, the filtered Green's function is less affected by many Lamb modes than non-filtered modes. In this case, the A0 flexible mode is the dominant mode overruling the wave shape of Green's function but still has oscillation due to S0 mode and A1 mode. Therefore, if the thickness of the laminate, H, is much smaller than the wavelength, then the problem can be solved by approximate SDPT. Fig. 6 shows the recovered force by deconvolving the simulated response signal into force and Green's function based on Eq. (35). They are completely corresponding. It is natural because it is a simulated signal.

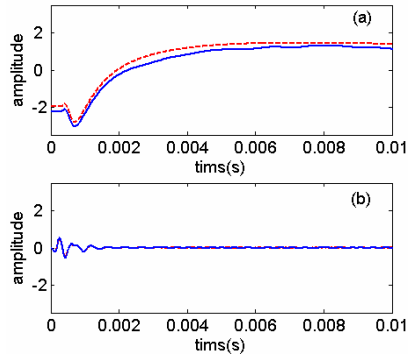

Fig. 4. shows the comparison between Green's function at r = 200 mm obtained by using exact solution and that by using SPDT in aluminum plate. Sampling frequency is 81920Hz (a) non-filtered Green's function (b) filtered Green's function with Butterworth band pass filter from 2,000Hz to 4,000Hz: (·····): Exact solution, (——): SDPT.

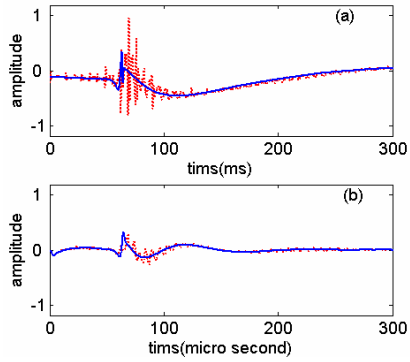

Fig. 5. shows the comparison between Green's function at r = 200 mm obtained by using exact solution and that by using SPDT in aluminum plate. Sampling frequency is 4,096,000Hz (a) non-filtered Green's function (b) filtered Green's function with Butterworth band pass filter from 10,000Hz to 200,000Hz. (·····): Exact solution, (——): SDPT.

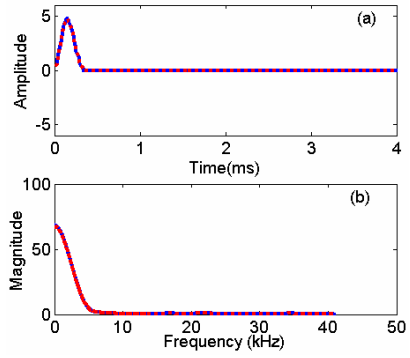

Fig. 6. Recovered force by deconvolving the simulated response signal into force and Green's function: (·····) True impact load, (——) Recovered impact load.

3. Theoretical and experimental validation for waveform

A schematic of the experimental setup is shown in Fig. 7 and Fig. 8. An aluminum plate was used, with dimensions 1200mm × 1200mm and 10mm. The impact load was excited by the impact hammer with aluminum tip. The model of impact hammer used for the test is ENDEVECO model 2302. Fig. 9 shows the sensor arrangement and location of the impact for the experiment. The accelerometers used to detect waves in the plate were B & K accelerometer type 4390. The outputs from the accelerometers were amplified by using the charge and signal conditioner of ENDEVECO model 133. The signals were then digitized with a TDS2034 color 4-channels digital oscilloscope at a sampling rate of 50kHz. Software for the data transfer from scope to the computer was supplied by Texas Instrument Company. When the impact hammer excites the impact position in the plate as shown in Fig. 9, the acceleration at positions S_0, S_1 and S_2 is measured by experiment. The theoretical displacements are obtained by using the approximate SDPT and their accelerations are calculated by double differentiation of those displacements. Because the cut-off frequency of the measured accelerations is 25kHz, the theoretical acceleration is also calculated up to 25kHz. The frequency resolutions in both of theoretical and experimental acceleration are 20Hz. The sampling ratio in both the theoretical and experimental acceleration is 50kHz. Fig. 10 shows the comparison between the simulated waveform using SDPT and measured waveform. The waveforms in the top line are non-filtered waves, and the waveforms in bottom are filtered waveforms. The measured waveforms show reflected wave, whilst the simulated waveform has only direct wave in infinite plate. The waveforms measured at sensor S_0 and sensor S_1 are affected more early by reflected wave than waveform measured at sensor S_2 since they are a far distance from the impact point and nearest to the edge of plate. In the region of direct wave, in order to remove the effect of a reflection wave, a band pass filter is used. After filtering, in the region of direct wave, the simulated waveforms are well corresponding with the measured waveforms. The spectrum of impact load $\hat{f}(\omega)$ used for the impact is shown in Fig. 11. In the reference [16], the impact force is inversely determined with waveforms measured only by the three sensors as shown in Fig. 7 and with the Green's function theoretically obtained by using the exact solution.

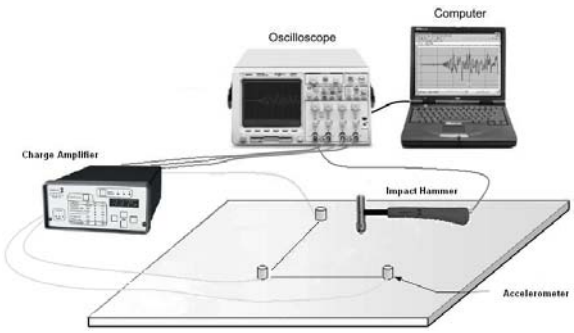

Fig. 7. Schematic of experimental setup.

Fig. 8. Schematic of experimental setup.

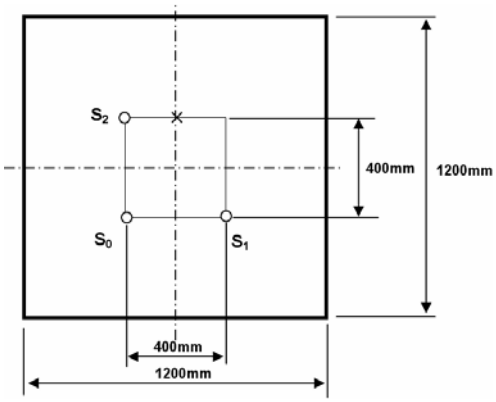

Fig. 9. Location of impact hammer and accelerometers. (S_0 = 447mm, S_1 = 447mm, S_2 = 200mm from Impact position).

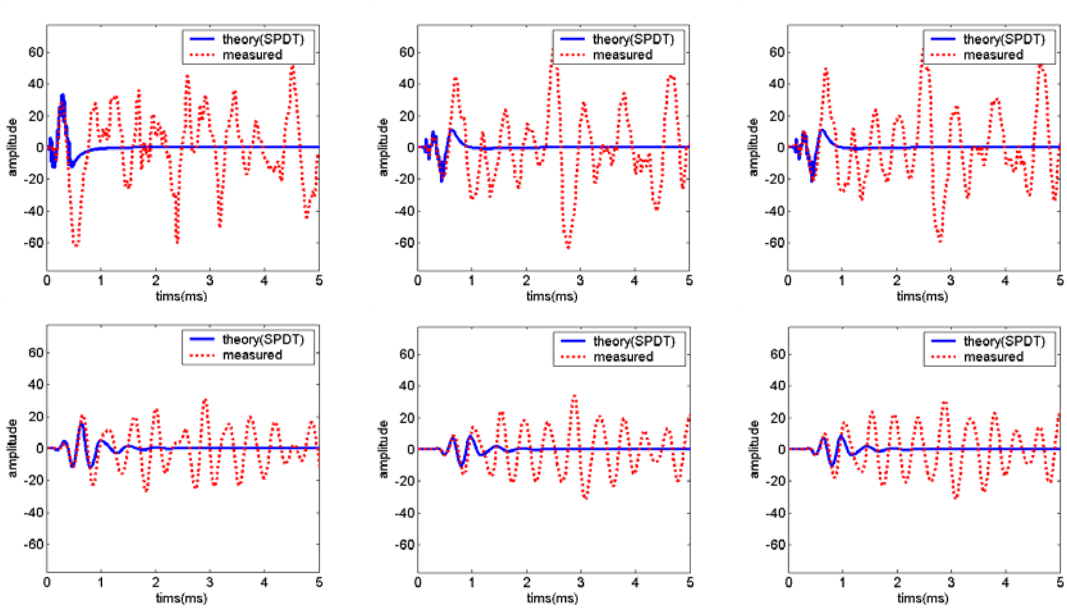

Fig. 10. Comparison between the simulated waveform using SDPT and measured waveform.

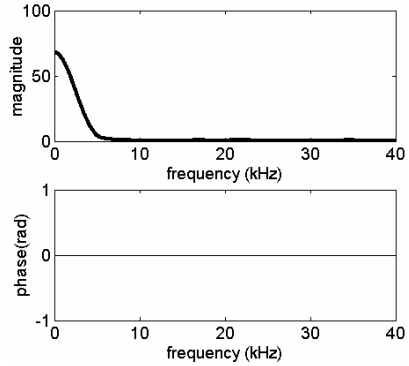

Fig. 11. Frequency spectrum of impact force measured throughout force transducer.

This is processed after determining the location of impact load.

4. Conclusion

The paper presents a method for the determining the impact load on the thick plate inversely based on Green's function and the waveform due to impact load at the arbitrary point on the surface of the plate. The waveform is theoretically calculated based on plate theory. The exact plate theory and the approximated shear deformation theory (SDPT) are employed instead of the CPT since the CPT overestimates the group velocity at high frequency in a thick plate. The estimated waveform very well corresponds with the experimental results and the impact load is inversely determined with theoretical Green's function.

Acknowledgments

Authors thank Prof. A. K. Mal in Mechanical Engineering and Aerospace Engineering Department, University of California, Los Angeles for his permission regarding electrodynamics software.

Reference

[1] J. E. Michaels and and Y. H. Pao, Determination of dynamic forces from wave motion measurements, *J. Appl. Mech*., 53 (1986) 61-68.

[2] L. Gaul and S. Hurlebaus, Determination of the impact force on a plate by piezoelectric film sensors, *Archiv. Appl. Mech*., 69 (1999) 691-701.

[3] C. S. Yen and E. Wu, On the inverse problem of rectangular plates subjected to elastic impact, part I: method development and numerical verification, *J. Appl. Mech.,* 62 (1995) 692-697.

[4] M. Tracy and F. K. Chang, Identifying impacts in composite plates with piezoelectric strain sensors, part I: Theory, *J. Intelligent Material System and Structures,* 9 (1998) 920-928.

[5] S. Banerjee and A. K. Mal, Analysis of transient Lamb waves generated by dynamic surface source in thin composite plates, *J. Acoust. Soc. Am.,* 115 (2004) 1905-1911.

[6] S. M. Ziola and M. R. Gorman, Source location in thin plates using cross-correlation, *J. Acoust. Soc. Am.,* 90 (1991) 2551-2556.

[7] K. Kishimoto, H. Inoue, M. Hamada and T. Shibuya, Time frequency analysis of dispersive waves by means of wavelet transform, *J. Appl. Mech.,* 62 (1995) 841-846.

[8] L. Gaul and S. Hurlebaus, Identification of the impact location a plate using wavelets, *Mech. Sys. Signal Process.,* 12 (1997) 783-795.

[9] R. D. Mindlin, Influence of rotatory inertia and shear flexural motion of isotropic, elastic plate, *J. Appl. Mech*., 18 (1951) 31-38.

[10] K. Mal and S. S. Lih, Elastodynamic response of a unidirectional composite laminate to concentrated surface loads: part I, *J. Appl. Mech*., 59 (1992) 878-886.

[11] S. S. Lih and A. K. Mal, On the accuracy of approximate plate theories for wave field calculations in composite laminates, *Wave Motion,* 21 (1995) 17-24.

[12] K. Mal, Y. Bar-Cohen and S. S. Lih, Wave attenuation in fiber-reinforced composites, International Conference on Mechanics and Mechanisms of Material Damping, ASTM STP 1169 (1992) 245-261.

[13] MA. K. Mal and S. Singh, Deformation of Elastic Solids, Prentice Hall, New Jersey, USA, (1991).

[14] K. Mal, Wave propagation in layered composite laminates under periodic surface loads, *Wave Motion,* 10 (1988) 257-266.

[15] K. F. Graff, Wave, *Motion in Elastic Solids*, Dover Publications Inc., New York, (1953).

[16] S. K. Lee, Identification of Impact Force in Thick Plates Based on the Elastodynamics and Time-Frequency Method (Part II: Experimental Approach for Identification the Impact Force Based on Time Frequency Methods), *The Journal of Mechanical Science and Technology*, Submitted paper, (2008).